Molecular dynamics simulations of hard sphere solidification at constant pressure

T. Gruhn and P. A. Monson
Department of Chemical Engineering, University of Massachusetts, Amherst, Massachusetts 01003
(Received 2 August 2001; published 20 November 2001)

Molecular dynamics simulations in the NPT ensemble are used to study the dynamics of crystallization processes in hard sphere systems. The simulation method used permits us to follow the dynamics after a sudden pressure or temperature quench in a one-step process without the need of extra densification methods. During the quench a strong correlation between the system density and the crystalline order parameter Q_6 is found. The growth of fcc order in the system over time is observed in detail and compared to $Q_6(t)$. We compare results for the equation of state on the metastable fluid branch with previous results from constant volume molecular dynamics simulations. Some results for the crystallization of binary hard sphere mixtures are also presented for a number of different size ratios.

DOI: 10.1103/PhysRevE.64.061703 PACS number(s): 61.30.Cz, 68.08.−p, 61.20.Ja, 68.35.Md

I. INTRODUCTION

The hard sphere potential is one of the most frequently and thoroughly investigated model potentials for molecular interactions. In spite of its simplicity it mimics surprisingly well the properties of simple fluids and colloidal suspensions. This is especially true at high densities, where the behavior of real fluids is mainly dictated by short range repulsive forces rather than longer ranged attractions. Since the first molecular dynamics (MD) simulations in the 1950's [1,2] the hard sphere potential has raised a number of interesting questions, some of which now appear to be answered while for others definitive conclusions are still lacking. First of all, the hard sphere system analysis revealed strong evidence for the existence of a first-order transition from a disordered to an ordered phase simply from short range repulsions [3–6]. Although it is quite clear that hard spheres have an ordered phase it took a long time and very careful investigations to estimate the most stable crystalline structure of hard spheres. A number of independent recent studies seem to show that the fcc structure has a slightly lower Helmholtz free energy than the hcp crystalline structure [7–11].

The various equilibrium states of one-component hard sphere systems can be depicted in a phase diagram showing $P_E\sigma^3/kT$ versus the volume fraction η. A branch of fluid equilibrium states starts from low densities and goes to a volume fraction of $\eta\approx 0.494$ while $P_E\sigma^3/kT$ increases from $P_E\sigma^3/kT=0$ to $P_E\sigma^3/kT\approx 11.59$, well described by the Carnahan-Starling equation [12]. A phase coexistence region with constant $P_E\sigma^3/kT\approx 11.59$ connects the freezing point at the end of the fluid branch with the melting point at $\eta\approx 0.545$ where the fcc solid branch starts [3,4]. On the solid branch the $P_E\sigma^3/kT$ value increases with increasing density and diverges at the close packed volume fraction of $\eta=\pi\sqrt{2}/6$. If a fluid hard sphere system is compressed beyond the freezing point it may follow a fourth branch consisting of metastable dense packed fluid states. It is assumed that the metastable branch ends at a volume fraction $\eta\approx 0.64$ where the corresponding $P_E\sigma^3/kT$ value diverges. This limit is often denoted as ''random close packing,'' although the existence of a well defined state of random close packing has been called into question in recent work [13].

Much recent attention has been paid to the dense packed metastable fluid states and the crystallization processes initiated from them [13–16,18–23].

For volume fractions $\eta<0.57$, metastable states are described quite well by the Carnahan-Starling equation. However, for volume fractions in the range $0.53<\eta<0.58$ the system easily starts to freeze and does not stay very long in a metastable fluid state [15,19,21]. With high compression rates metastable fluid states with volume fractions higher than 0.58 can be reached. Metastable states with $\eta\geqslant 0.57$ can be fitted nicely by a phenomenological equation of state

$$P_EV/NkT=A/(1-\eta/\eta_g),\quad 0.57\geqslant\eta<\eta_g \qquad (1.1)$$

with $A=2.67$ and $\eta_g=0.648$ proposed by Speedy [14]. He suggests that at $\eta\approx 0.57$ a second-order phase transition occurs from a metastable fluid to a glassy state. However the region around $\eta\approx 0.57$ is difficult to analyze. Slow compressions lead to crystallization while for high compression rates a number of glasses with individual branches were observed [19]. A quickly compressed system might get stuck at a nonideal glassy state, i.e., on a fluidlike state that does not have the lowest possible pressure for the respective volume fraction. Rintoul and Torquato dispute the existence of a thermodynamic glass transition [15–17]. They propose that crystallization can start from any metastable state though for high densities it might take a very long time and especially small systems might get frustrated by finite size effects. They claim that signs of crystallization are found for all densities if the system is chosen large enough. This is in contradiction with other observations that find that small systems crystallize faster than large ones [18,21,23]. Further analysis of the crystallization process was done by Richard *et al.* [21] while special attention to the time development of different types of crystalline order was paid by Kendall *et al.* [23].

Computer simulation studies of the thermodynamics of hard sphere solids have been extended to mixtures [24–27]. In addition to the formation of binary alloys without substitutional order, substitutionally ordered solid phases like AB, AB_2 or AB_{13} can form, depending on the chosen size ratio $\alpha=r_B/r_A$ of the components A and B. The stability of those

phases has recently been investigated in computer simulations [25–27]. Quantitatively accurate theoretical predictions have also been made [28].

Much less attention has been devoted to the crystallization process in binary hard sphere mixtures. Jackson *et al.* [29] provided evidence of crystallization from Monte Carlo and MD simulations for several size ratios, but at the time of their work there had yet to be accurate calculations of the solid-fluid phase diagrams. Eldridge *et al.* [25] have compared the phase diagrams obtained from computer simulations with experimental results. They find that in experiments for size ratios between $0.5 \leqslant \alpha \leqslant 0.625$ AB_{13} is found more often than expected from the phase diagrams. They argue that during the crystallization process in the fluid phase the formation of icosahedral order is strongly favored so that it is likely that a metastable AB_{13} phase forms in the experiment since the small spheres in the AB_{13} phase show icosahedral order. In a MD simulation where the volume is continuously reduced, they find that fcc and icosahedral order increases but they do not see crystallization at the compression rates they used. Trizac and coworkers describe a simulation that starts from a metastable AB structure at a phase point where an A crystal coexists with a fluid AB mixture [27]. As predicted from theory, they observe a phase separation: In some parts of the system the B component escapes from the crystal structure that becomes a pure A crystal while the rest of the simulation box is filled with a mixture of the A and B components.

Up to now molecular dynamics simulations of crystallization processes in hard sphere systems have been restricted to the NVE ensemble, where the number of molecules N, the volume V, and the total energy E is kept fixed. Crystallization is induced by a density quenching process for which a number of sophisticated densification methods [14, 30–32] have been developed. They all perform a series of small density increments while the spheres are moved such that overlaps are avoided. The methods are typically optimized to produce rather high densities with rather low degree of order in a rather low amount of CPU time and are not basically intended to simulate the dynamics that might be found in real systems. Structural properties of the resulting dense metastable fluids depend on the densification method. It is unclear how much the behavior of a subsequent NVE simulation is influenced by the artificial compression methods used to generate the high density fluid states. In this paper we present an application to this problem of a molecular dynamics simulation method for hard sphere systems in the NPT ensemble, where the external pressure P_E, the number of spheres N and the temperature T is kept fixed. This method allows us to replace the two-step process of densifying a low density system and then applying NVE molecular dynamics by one continuous NPT simulation that traces the development of a highly ordered dense state from a low density fluid state.

Molecular dynamics simulations at a constant pressure have become a standard method for the computational investigation of soft potential model systems [33,34]. Soft potential fluids in the NPH ensemble, in which a system of N molecules in a fluctuating volume V is exposed to a constant pressure P_E at a constant enthalpy $H=U+P_EV$, are typically studied by a method originally introduced by Andersen [35]. In 1986 de Smedt *et al.* [36] described an adaptation of the Andersen algorithm to hard sphere systems in ν dimensions. In a recent paper [37] we presented an implementation of the de Smedt analysis and demonstrated its accuracy. One finds that for a hard sphere system in the NPH ensemble a one-step crystallization process starting from a low density fluid is impossible [37]. Thus we modified the de Smedt method to enable NPT ensemble simulations which are more suitable for crystallization. Accuracy tests of the NPT algorithm were also presented in Ref. [37].

The purpose of this paper is to describe the application of constant pressure molecular dynamics to crystallization in hard sphere systems, including the case of binary mixtures. For single component systems, simulations are performed for various values of P_E/T starting from a low density fluid state. During the simulation run the system increases in density. Depending on the chosen value of P_E/T the system might end up in a metastable fluid state or crystallization may set in. The fluctuating volume allows changes of the system's state that may otherwise be strongly hindered by free energy barriers or that may be prevented if the phase space is really divided into isolated glasses. During the crystallization process, the time development of the system density, the degree of crystalline order, and the degree of fcc order is analyzed at constant pressure. The mutual dependence of these quantities is investigated and used to identify the metastable fluid states at a given pressure. The results are compared to those from previous NVE ensemble simulations. We apply a similar procedure to study the crystallization of several binary mixtures for several size ratios and compositions.

The remainder of this paper is organized as follows. In Sec. II a short description of the algorithm is given together with an introduction of the used order parameters. Technical details of the simulation are given in Sec. III. Section IV is devoted to the presentation of the results and in Sec. V summary and conclusions are given.

II. THEORETICAL BACKGROUND

The algorithm used in the present work is described in detail in Ref. [37]. In general, molecular dynamics simulations of hard sphere systems consist of three fundamental steps: (i) estimation of collision times; (ii) propagation of the system towards the next collision event; and (iii) calculation of the impact of the collision upon the system. For convenience we review the essential aspects of how these three steps are implemented in the constant pressure algorithm.

A. The algorithm

We consider a system of N hard spheres i with masses m_i and coordinates $\mathbf{r}_i$. The system is situated in a cubic simulation box with periodic boundary conditions. In the NPH and the NPT ensembles the volume V of the cube is a dynamical variable and the coordinates are expressed in reduced form, $V^{1/3}\mathbf{q}_i \equiv \mathbf{r}_i$.

Following Andersen [35], we use the Lagrangian

$$L=\frac{V^{2/3}}{2}\sum_{i=1}^{N} m_i\dot{\mathbf{q}}_i\cdot\dot{\mathbf{q}}_i-U(\ldots,V^{1/3}\mathbf{q}_i,\ldots)+\frac{1}{2}M\dot{V}^2-P_EV, \tag{2.1}$$

where P_E is the external pressure and M is a system parameter, which determines the dynamics of the volume change. The spheres interact with each other via the hard sphere potential that assumes that molecules perform hard elastic collisions at a distance σ that for mixtures is typically chosen to be $\sigma=1/2(\sigma_i+\sigma_j)$.

1. Motion between two collisions

Between two collisions the potential $U(\ldots,V^{1/3}\mathbf{q}_i,\ldots)$ in Eq. (2.1) is zero. From the Lagrangian equations

$$m_i\ddot{\mathbf{q}}_i=-2m_i\dot{\mathbf{q}}_i\frac{\dot{V}}{3V}\qquad(i=1,\ldots,N) \tag{2.2}$$

$$M\ddot{V}=\frac{1}{3V^{1/3}}\sum_i m_i\dot{\mathbf{q}}_i^2-P_E, \tag{2.3}$$

which form a set of $3N+1$ coupled differential equations, one differential equation for the volume can be extracted,

$$\ddot{V}(t)=\frac{2C}{3M}V^{-5/3}(t)-\frac{P_E}{M}. \tag{2.4}$$

Here the constant

$$C\equiv V_0^{4/3}\sum_i\frac{m_i}{2}(\dot{q}_i^0)^2 \tag{2.5}$$

depends on $V_0\equiv V(t_0)$ and $\dot{q}_i^0\equiv\dot{q}_i(t_0)$ at the beginning t_0 of the considered time interval.

Since there is no closed form expression for the analytical solution of Eq. (2.4) we integrate Eq. (2.4) numerically by using a velocity-Verlet-like approximation [33] for small time steps $\tilde{t}=t-t_0$,

$$V(t)\approx V(t_0)+\dot{V}(t_0)\tilde{t}+\frac{1}{2}\ddot{V}(t_0)\tilde{t}^2$$

$$\dot{V}(t)\approx\dot{V}(t_0)+\frac{1}{2}\tilde{t}[\ddot{V}(t_0)+\ddot{V}(t)]. \tag{2.6}$$

Here the second derivative of V is given by Eq. (2.4).

From Eq. (2.2) one has

$$\dot{\mathbf{q}}_i(t)=\kappa_iV^{-2/3}(t)\quad\text{with }\kappa_i\equiv\dot{\mathbf{q}}_i(t_0)V^{2/3}(t_0). \tag{2.7}$$

For small $\tilde{t}$ the unscaled coordinates $q_i(t)$ themselves can be estimated by a Taylor expansion

$$\mathbf{q}_i^1\approx\mathbf{q}_i^0+\dot{\mathbf{q}}_i(t_0)\tilde{t}+\frac{1}{2}\ddot{\mathbf{q}}_i(t_0)\tilde{t}^2=\mathbf{q}_i^0+\dot{\mathbf{q}}_i(t_0)\tilde{t}-\dot{\mathbf{q}}_i(t_0)\frac{\dot{V}_0}{3V_0}\tilde{t}^2. \tag{2.8}$$

2. Estimating the next collision time

If the next collision between two hard spheres occurs at a time t_1 that is not too far from t_0 the system can be propagated directly to t_1. A pair of molecules i and j collides if the relation

$$V^{2/3}(t_c)\|\mathbf{q}_{ij}\|^2(t_c)=\sigma^2 \tag{2.9}$$

with $\mathbf{q}_{ij}=\mathbf{q}_j-\mathbf{q}_i$ is fulfilled. A second-order Taylor approximation for the left hand side of Eq. (2.9) leads to a quadratic function for t_c in which all parameters are determined from the discretized equations of motion.

3. Collision behavior

The hard sphere collision behavior in the NPH ensemble can be taken from Ref. [36]. For two colliding spheres i and j with reduced coordinates $\mathbf{q}_i$ and $\mathbf{q}_j$ and reduced velocities $\dot{\mathbf{q}}_i$ and $\dot{\mathbf{q}}_j$ one gets

$$\mathbf{q}=\mathbf{q}_j-\mathbf{q}_i\quad\Delta\dot{\mathbf{q}}_j=\frac{\overline{t_d}}{m_j\sigma}\mathbf{q},$$

$$\dot{q}^b=\sigma^{-1}V^{1/3}(\dot{\mathbf{q}}_j^b-\dot{\mathbf{q}}_i^b)\cdot\mathbf{q}\quad\Delta\dot{\mathbf{q}}_i=-\frac{\overline{t_d}}{m_i\sigma}\mathbf{q},$$

$$\overline{t_d}=-\frac{2\mu\left[V^{1/3}\dot{q}^b+\sigma\dfrac{\dot{V}^b}{3V}\right]}{1+\dfrac{\mu\sigma^2}{9MV^2}}\quad\Delta\dot{V}=\frac{\sigma\overline{t_d}}{3MV}.$$

B. Hard spheres in the *NPT* ensemble

The algorithm described above correctly yields the hard sphere system dynamics in the NPH ensemble (see Ref. [37]). However, in experiments typically the temperature is kept constant rather than the enthalpy so that an NPT simulation is closer to the typical conditions in a freezing process. Moreover, the constant enthalpy H in the NPH ensemble leads to the equation

$$\text{const}=H=E+P_EV=\frac{3N-2}{2}kT+P_EV, \tag{2.10}$$

which for large N leads to a hyperbolic relation between the fluctuating quantities P_E/T and ρ,

$$\frac{H}{NP_E}=\frac{3}{2}\left(\frac{P_E}{kT}\right)^{-1}+\rho^{-1}\quad(N\to\infty). \tag{2.11}$$

For the melting point with $P_E\sigma^3/kT\approx11.59$ and $\rho\sigma^3\approx1.041$ one has

$$\frac{H}{NP_E} \approx 1.09\sigma^3 \approx \frac{1}{0.92}\sigma^3. \tag{2.12}$$

Since the left hand side remains constant in the NPH ensemble neither the melting point nor any other solid state point can be reached from an initial fluid state with a density lower than $\rho\sigma^3 < 0.92$. This is a big disadvantage for the investigation of crystallization processes, because $\rho\sigma^3 = 0.92$ corresponds to a very dense fluid state with a high degree of local order.

For all these reasons NPT ensemble simulations are preferable to NPH simulations for the study of quenching processes. If one starts with the Lagrangian equations introduced by Nosé, one can easily derive equations of motion for the NPT ensemble of hard spheres but the implementation is very CPU time consuming so that appropriate system sizes and sufficiently long simulation runs become impractical. Therefore, we used the same algorithm as derived for the NPH ensemble and added a velocity rescaling step after each time propagation so that

$$\text{const} = kT = \frac{2}{3(N-1)+1}\left(\sum_{i=1}^{N}\frac{m_i}{2}V^{2/3}\dot{\mathbf{q}}_i^2 + \frac{M}{2}\dot{V}^2\right). \tag{2.13}$$

Tests that demonstrate the accuracy of this *ad hoc* algorithm are reported in Ref. [37].

C. Crystalline order parameters

Although the interpretations of the metastable fluid branch may vary, the observed simulation results from different research groups appear to match very well over the investigated density region. Generally one could describe the metastable fluid branch as the set of state points (η, P) each having the following properties: (1a) The volume fraction η is larger than the freezing volume fraction η_{cryst}; (1b) For a given η the pressure P is the lowest pressure for which the system does not show crystalline order. Equivalently the state points can be characterized by the properties: (2a) The pressure P is larger than the freezing pressure $P(\eta_{cryst})$; (2b) For the given pressure the volume fraction η is the highest volume fraction for which the system does not show crystalline order. These characterizations imply that there is a criterion for the existence of crystalline order in the system. A macroscopic crystalline state is characterized by a three-dimensional long range spatial order. During the crystallization process, however, parts of the system might show local crystalline order while others are still fluid. The principal axes of the developing crystalline order are generally oriented randomly. Several methods have been developed to detect crystalline order in a system and to quantify the degree of crystalline order for a cluster of molecules. Some information can be extracted from the radial distribution function $g(r)$. The appearance of crystalline order is reflected in characteristic peaks and shoulders in $g(r)$, but these indicators may not be clear if the degree of crystalline order is low [15]. The local crystalline order can also be specified by analyzing the (modified) Voronoi polyhedron around a molecule in the system [38,39]. Unfortunately, this method is not very helpful for the important case of fcc order, where small fluctuations of the local order lead to strong topological changes in the Voronoi polyhedra.

TABLE I. Values of Q_6 for different cluster types.

Cluster type	Q_6
Icosaeder	0.66332
Fcc	0.57452
Hcp	0.48476
Bcc	0.51059
Simple cubic	0.35355
Random order	0.00000

Another approach is based on the correlation of bond vectors $\mathbf{r}$ between a molecule of choice and its neighbors [40,41]. The set of neighbor molecules can be defined as all molecules within a cut-off radius around the central molecule, or the K closest molecules or molecules whose Voronoi polyhedron shares a polygon with the polyhedron of the central molecule. In the following a cut-off radius was used to determine the neighbors. Crystalline order parameters can then be defined with the help of spherical harmonics

$$Q_{lm}(\mathbf{r}) = Y_{lm}(\theta(\mathbf{r}), \phi(\mathbf{r})). \tag{2.14}$$

These quantities are dependent on the choice of the coordinate frame. One can form second-order invariants

$$Q_l = \left(\frac{4\pi}{2l+1}\sum_{m=-l}^{l}|\overline{Q_{lm}}|^2\right)^{1/2}, \tag{2.15}$$

where the bar denotes the average over all neighbors of the considered molecule. It was found that Q_6 is a very sensitive parameter for overall crystalline order [15,16,21]. For an infinite and perfectly disordered fluid system $Q_6 = 0$. For finite systems Q_6 gives a small finite value due to thermal fluctuations. For fcc, bcc, hcp, and simple cubic crystals, Q_6 is distinctly larger than zero as shown in Table I.

More detailed information about the local crystalline order can be extracted from the third-order invariants [42]

$$Q_{l_1 l_2 l_3} = \sum_{m_1+m_2+m_3=0}\begin{pmatrix} l_1 & l_2 & l_3 \\ m_1 & m_2 & m_3 \end{pmatrix} Y_{l_1 m_1} Y_{l_2 m_2} Y_{l_3 m_3}. \tag{2.16}$$

An extremely useful indicator for fcc clusters is Q_{446}. In a histogram of Q_{446} fcc clusters form a peak around $Q_{446} = 2.5\times 10^{-3}$ that is well separated from a second peak around $Q_{446} = 0$ formed by all other symmetries of clusters. As suggested in Ref. [42] one can declare a cluster to be fcc-like if its value of Q_{446} is larger than $Q_{446} > 0.0007$ which approximately corresponds to the minimum between the two peaks.

III. SIMULATION PROCEDURE

Our first goal is the analysis of the dynamical behavior of one-component hard sphere systems subjected to a sudden quench caused by an abrupt increase of the external pressure P_E.

In most cases one-component systems were investigated with $N=2048$ spheres. Comparative simulations with $N=864$ spheres did not show essential size effects beside a faster crystallization of the latter systems. A number of binary mixture simulations were then performed with $N=864$ spheres. A maximum time propagation step of $t^*_{max}=10^{-4}$ in units of $\sigma\sqrt{m/kT}$ was set to ensure that the calculation error for the next collision time of spheres remains acceptably small.

At the beginning of each one-component system run, a random fluid state is created by relaxing an fcc ordered system with an external pressure of $P_E\sigma^3/kT=2.0$ over a time period of $t_{relax}=4\times10^6 t_{max}$ during which about 1.4×10^6 collisions took place. After the relaxation time the system has reached the equilibrium density $\rho\sigma^3=0.285$ in accord with the Carnahan-Starling equation and the radial distribution function matches the results from a corresponding Monte Carlo simulation in the NVT ensemble. The crystalline order parameter levels off to a finite value between 0.01 and 0.02 which is a size effect of the finite system with $N=2048$ particles. After the relaxation process the pressure is increased to the value of interest and the time development of the system is investigated.

For the binary mixtures simulations were started with $P_E\sigma^3_{AA}/kT=2.0$ where σ_{AA} is the contact distance of two A component spheres. Accordingly σ_{AB} and σ_{BB} denote the contact distance of an A and a B sphere and the contact distance of two B spheres, respectively. At the beginning of the simulations the two species were distributed randomly on fcc lattice sites. After the initial equilibration time with $P_E\sigma^3_{AA}/kT=2.0$ the fluid character of the system was checked as described for the one-component systems.

IV. RESULTS

A. One-component systems

As we mentioned in the Introduction, in previous work crystallization processes and the metastable branch of hard sphere one-component systems were investigated in the NVE ensemble where the total energy and the density of the system is constant [15,16,22,23]. To set up such simulations a densification algorithm is applied on a low density fluid state (see Ref. [30–32,14]). These algorithms typically produce high density states with a pressure higher than that of the metastable branch. As the MD simulation is started, an equilibration process sets in. At constant density the pressure diminishes as the system approaches the metastable branch. This relaxation process may have superimposed upon it a crystallization process that drives the system from the metastable branch towards the stable solid branch. If relaxation and crystallization times are of the same order of magnitude, the determination of the pressure value for the metastable branch becomes difficult.

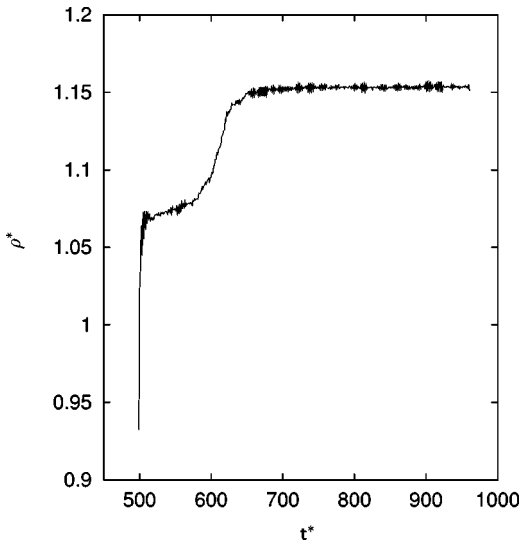

FIG. 1. Typical example of the time dependence of the reduced density $\rho^*=\rho\sigma^3$ as a function of time $t^*=t/(\sigma\sqrt{m/kT})$ for $P_E\sigma^3/(kT)=22.0$.

In NPT molecular dynamics simulations the pressure P_E is an external parameter. If the external pressure for a low density fluid hard sphere system is increased in a one-step process, the system responds with a rapid increase of the density. Afterwards the time dependence of the density varies from each individual run to the next, but qualitative similarities are found for the different $\rho(t)$ obtained in various runs of systems with $N=2048$, 864, and 128. In Fig. 1 a typical example for the time dependence of the density of an initially dilute fluid state is shown for $P_E\sigma^3/kT=22$. There is a steep increase of the density until a value of about $\rho\sigma^3\approx1.06$ is reached. From there the average density increases very slowly before another rapid increase of the density sets in that ends at $\rho\sigma^3\approx1.155$. At this value the density remains until the end of the simulation run. The intermediate time interval with the slowly rising density $\rho(t)$ is reminiscent of the decrease in $P_E(t)$ in NVE simulations around the metastable state. In some simulation runs the increase of $\rho(t)$ after the first plateau took place in two or more steps.

For a more detailed picture, it is helpful to consider the crystalline order parameter. A plot of $Q_6(t)$ as a function of time is given in Fig. 2. It starts with a slow increase from $Q_6\approx0.02$ to $Q_6\approx0.07$ spanning the time interval where also $\rho(t)$ has a small slope. Then abruptly a fast increase of Q_6 sets in that ends at $Q_6\approx0.46$ beyond which the crystalline order increases only slightly.

Though the functions $\rho(t)$ and $Q_6(t)$ were varying with each simulation run there was always a striking correlation between the time behavior of the two quantities in each individual run. Thus it is worthwhile to plot Q_6 as a function of ρ. This is done in Fig. 3 for three independent runs with $P_E\sigma^3/kT=22$. Evidently the three curves match well within the statistical fluctuations. Apparently there is a well defined value for ρ beyond which the order parameter abruptly begins to grow. This value of ρ coincides with the metastable state at the given pressure [14,16,21]. If we reconsider the time dependence of $\rho(t)$ and $Q_6(t)$ it turns out that the meta-

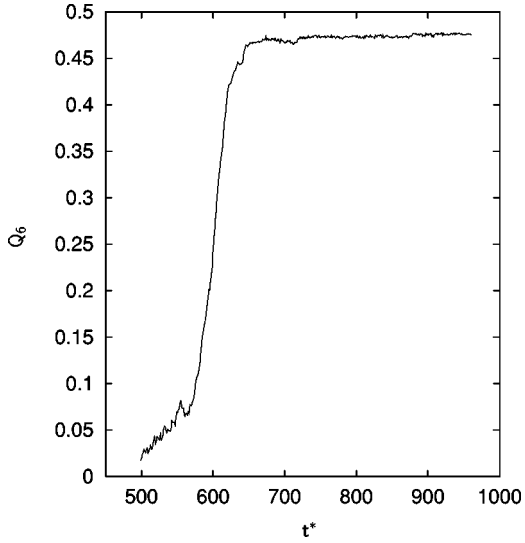

FIG. 2. Time dependence of the crystalline order parameter Q_6 as a function of time $t^*=t/(\sigma\sqrt{m/kT})$ for the same simulation run as was used for Fig. 1 with $P_E\sigma^3/(kT)=22.0$.

stable state corresponds to the starting point of the slow increase in ρ shown in Fig. 1.

It is an open question whether crystallization sets in for all densities below the random close packing value of $\rho\approx 0.64$ or if beyond a certain density the metastable branch consists of glassy states at which crystallization processes are completely absent. Rintoul and Torquato [15,16] observed small signs of crystallization even for high densities while Richard *et al.* [21] present a curve of Q_6 values over the volume fraction η after 10^9 collisions, which is almost zero not only for small volume fractions but also for volume fractions

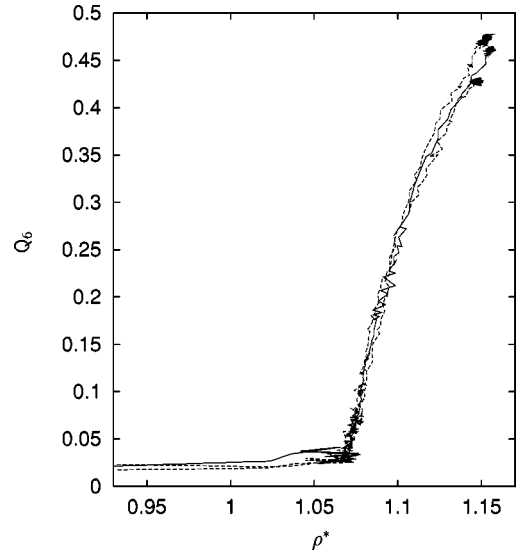

FIG. 3. Crystalline order parameter Q_6 as a function of the reduced density $\rho^*=\rho\sigma^3$ taken from three individual simulation runs with $P_E\sigma^3/(kT)=22.0$. Substantial crystalline order is found for densities higher than $\rho^*_{meta}\approx 1.076$ that coincides with the dense fluid metastable state. The finite value of Q_6 for densities below ρ^*_{meta} is caused by finite size effects.

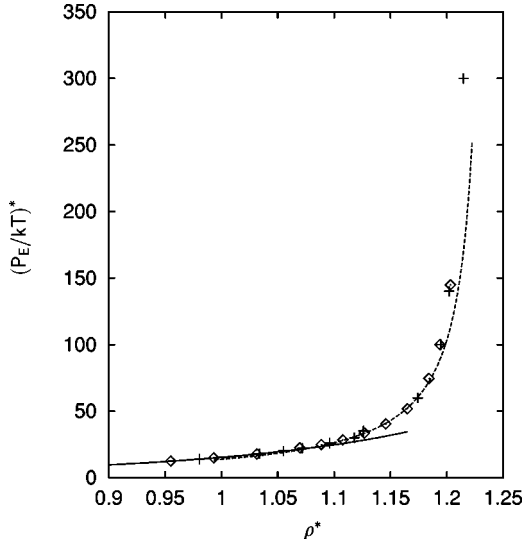

FIG. 4. Reduced pressure $(P/kT)^*=P_E\sigma^3/kT$ versus the reduced density $\rho^*=\rho\sigma^3$ for dense metastable fluid states. Results from NPT simulations (+) are extracted from individual runs at constant pressure. For comparison the figure shows results from NVE ensemble simulations [16] ($\diamond$), the Carnahan-Starling equation [12] continued beyond the freezing point (—), and a phenomenological equation proposed by Speedy (- - -) [see Eq. (1.1)].

larger than $\eta=0.6$. In other words in their NVE ensemble simulations they observe crystallization for volume fractions $0.56\leqslant\eta\leqslant 0.6$. Speedy reports that crystallization takes place in the region $0.53\leqslant\eta\leqslant 0.58$ [19]. It is interesting to note that Richard *et al.* as well as Speedy observe crystallization for volume fractions above the putative thermodynamic glass transition $\eta\approx 0.57$ since a crystallization of a real glass should, in principle, be impossible. One may argue, however, that crystallization has already set in during the densification process. In our NPT ensemble simulations crystallization was frequently found in the interval $20.0\leqslant P_E\sigma^3/kT\leqslant 30.0$. The corresponding volume fractions for the metastable states lie in the interval $0.55\leqslant\eta\leqslant 0.58$. In some cases crystallization was found for pressures up to $P_E\sigma^3/kT=50.0$ corresponding to the metastable state $\eta=0.6$.

In Fig. 4 metastable states obtained in NPT ensemble simulations are presented. In the crystallization region the values were obtained by determining the value of ρ beyond which Q_6 increases rapidly with ρ (see Fig. 3). For pressure values for which no crystallization occurred, an average of the density was taken after the equilibration of the system has come to an end, that is after systematic drifts of the density have stopped. Our data is in good agreement with results published by other groups, although it does show a somewhat larger scatter. For comparison, results of Rintoul and Torquato [16] are also shown in Fig. 4. For volume fractions up to $\eta<0.57$ and for $0.57\leqslant\eta\leqslant 1.18$ the simulation data are described well by the Carnahan-Starling equation and the phenomenological expression Eq. (1.1), respectively. As mentioned by Speedy, this on its own is not necessarily a proof of the existence of a second-order transition since the data can be described equally well by a con-

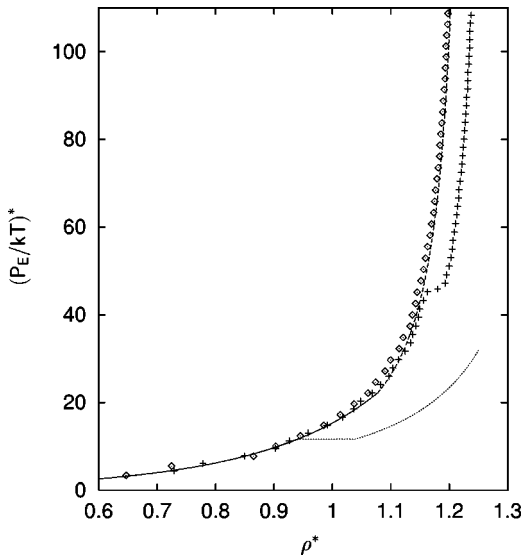

FIG. 5. Reduced pressure $(P/kT)^*=P_E\sigma^3/kT$ versus the reduced density, $\rho^*=\rho\sigma^3$, for dense metastable fluid states from NPT simulations with a linearly increasing pressure. Results are shown for pressure increment rates $(dP/dt)^*=0.5(+)$ and $(dP/dt)^*=2.0$ $(\diamond)$. Further the Carnahan-Starling equation [12] (—), the Eq. (1.1) by Speedy for metastable fluid states (- - -), and the stable branch beyond the freezing point $(\cdots)$ are shown.

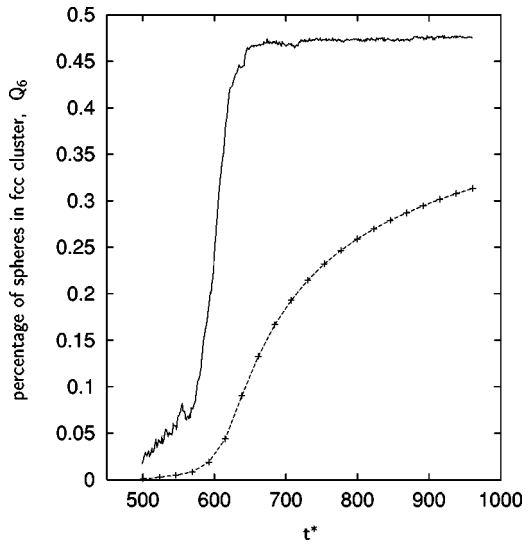

FIG. 6. Fraction of spheres in fcc clusters (- - - + - - -) compared to the crystalline order parameter Q_6 (—) as a function of time $t^*=t/(\sigma\sqrt{m/kT})$ for the same simulation run with $P_E\sigma^3/(kT)=22.0$.

tinuous function [14]. For large pressures the observed packing fractions are lower than those from Eq. (1.1). It is possible that this discrepancy is due to an unfinished relaxation process.

We have also made some studies where the pressure was increased steadily in the simulations rather than in a single quench. Studies were performed for various compression rates between $(dP/dt)^*=0.1$ and $(dP_E/dt)^*=2.0$. Results for the pressure versus density for two compression rates $(dP_E/dt)^*=0.5$ and $(dP_E/dt)^*=2.0$ are shown in Fig. 5. For $(dP_E/dt)^*=2.0$ no crystalline order was found up to a pressure of $(P_E/kT)^*=500.0$. As the pressure increases the density approximately follows the metastable branch although a small systematic deviation towards lower densities is noticeable. This is expected for high compression rates where the equilibration process lags behind the compression process. For $(dP_E/dt)^*=2.0$ the deviation from the Carnahan-Starling equation or Eq. (1.1) is always smaller than 1.5%. The highest deviation is found for pressure values around $(P_E/kT)^*=20.0$ while for $50.0<(P_E/kT)^*<500.0$ the density deviation is smaller than 0.6%. With lower compression rates the noncrystallized states get closer to the metastable branch, while the crystallization probability for $20.0\lesssim(P_E/kT)^*\lesssim50.0$ increases. The dynamics of the crystallization depends individually on the starting conditions but some characteristics can be extracted. The results in Fig. 5 with $(dP_E/dt)^*=0.5$ are a good example of the behavior. The values are close to the metastable branch up to a pressure of $(P_E/kT)^*\approx46$ where a distinct additional densification takes place. It is inviting to assume that the crystallization process starts spontaneously at that pressure value but we find that Q_6 increases steadily from $Q_6\approx0.06$ at $(P_E/kT)^*\approx24$ up to a value of $Q_6\approx0.26$ at $(P_E/kT)^*\approx46$ where it gets an additional increase to a value of $Q_6\approx0.34$. Systems staying close to the metastable branch with slowly growing crystalline order were found in several individual runs. However, for very low compression rates $(dP_E/dt)^*\lesssim0.2$ substantial crystallization already sets in at pressures $(P_E/kT)^*\approx20$ and the state points deviate immediately from the metastable branch. Generally, the observed phenomena are in qualitative agreement with observations made with densification algorithms for NVE ensemble simulations [14].

Development of fcc order

In the preceding section the typical crystallization dynamics in the NPT ensemble was described. As soon as the system approaches the metastable branch there is a slow steady increase of the crystalline order Q_6 before, rather abruptly, a strong increase of crystalline order sets in, which typically ends as abruptly as it begins. As mentioned above, Q_6 is an indicator for any sort of crystalline order without regard to the particular symmetry. With the help of Q_{446} histograms one can determine the quantity N_{fcc}/N that gives the fraction of spheres that are within an fcc cluster. Figure 6 shows a typical example of the time dependence of Q_6 and that of N_{fcc}/N for $P_E\sigma^3/kT=22$. It is evident that the amount of fcc order in the system increases more gradually with time than does Q_6. At the point where the sudden growth of $Q_6(t^*)$ terminates, $(N_{fcc}/N)(t^*)$ is still increasing. Thus, in the NPT ensemble, the system, starting from a metastable fluid state, begins to crystallize in a rather sudden process in which the density and the overall crystalline order parameter Q_6 increase rapidly. At the same time a process of fcc cluster development sets in. When the densification of the system has come to an end the amount of fcc order continues to increase. This motivates the following picture of the crys-

TABLE II. Reduced equilibrium density $\rho\sigma_{AA}^3$ obtained from NPT simulations of binary hard sphere mixtures with the given size ratio α, mole fraction x_A, and reduced pressure $P_E\sigma_{AA}^3/(kT)$. Results are compared with the extended Carnahan-Starling equation by Mansoori and coworkers [43].

α	x_A	$P_E\sigma_{AA}^3/(kT)$	$\rho\sigma_{AA}^3$ NPT simulation	$\rho\sigma_{AA}^3$ Mansoori eq.
0.6	0.25	3.0	1.108	1.109
0.6	0.25	6.0	1.482	1.486
0.6	0.25	9.0	1.713	1.715
0.6	0.5	3.0	0.887	0.889
0.6	0.5	6.0	1.151	1.149
0.6	0.5	9.0	1.306	1.303
0.6	0.75	3.0	0.741	0.741
0.6	0.75	6.0	0.937	0.939
0.6	0.75	9.0	1.054	1.054
0.8	0.25	3.0	0.845	0.846
0.8	0.25	6.0	1.093	1.093
0.8	0.25	9.0	1.237	1.239

tallization process. Due to the pressure the system approaches the metastable state, where, for a certain time a further densification is hindered. The system rearranges its configuration until a further densification is possible. As soon as parts of the system become more compact the whole system starts to give way to approach a new configuration with a distinctly higher density. The new state includes clusters of high density and a correspondingly high degree of crystallization order, while the crystal type of each cluster depends on the individual initial configuration. Now, with a distinctly slower dynamics fcc clusters rearrange and aggregate to form larger fcc clusters. Interestingly this process does not lead to a further noticeable increase of the density nor to an essential increase of the Q_6 order parameter. This mechanism was qualitatively reproduced in several individual runs for various system sizes. However, the final value of N_{fcc}/N strongly varied with each individual run.

B. Mixtures

The algorithm we are using [37] is already suited to run NPT molecular dynamics simulations for systems of hard sphere mixtures. However, to check the accuracy, a number of fluid equilibrium states were simulated and compared with predictions of the accurate equation of state for hard sphere systems [43]. A comparison of results is shown in Table II. The discrepancy is never larger than 0.3%.

As mentioned in the Introduction, there is only a small number of papers in which crystallization processes of hard sphere mixture systems have been investigated. This is not too surprising since the crystallization process is strongly hindered by the presence of more than one component. In fact mixtures have been used to study the metastable state just because of their tendency to stay fluidlike at conditions where a one-component system would crystallize [19].

It is reasonable to expect that the crystallization behavior is not too different from the pure component case if the size ratio α is close to 1. As an example we present the results for a low density binary mixture fluid with $\alpha=0.95$ and a mole fraction $x_A=0.7$ that is quenched to a pressure of $P_E\sigma_{AA}^3/kT=26$ in comparison with results from a corresponding one-component system quench for the A spheres at the same pressure. The radial distribution functions $g_{AA}(r)$, $g_{AB}(r)$, and $g_{BB}(r)$, which are shown in Fig. 7, are very similar indicating that the two components form a shared crystal with substitutional disorder. The locations of the maxima of the respective plots never deviate more than $0.025\sigma_A$ up to the eighth maximum. All these agree closely with the $g(r)$ function of the quenched and crystallized one-component system (Fig. 7). However, for the one-component $g(r)$ maxima are shifted slightly but systematically towards higher values of r. At the eighth peak the discrepancy becomes $0.05\sigma_A$. Interestingly, for large r the peaks in the pair distribution function for the mixture are slightly more pronounced than those for the one-component system although the mixture ends up with a lower degree of order than the pure hard sphere system as is shown in Fig. 8.

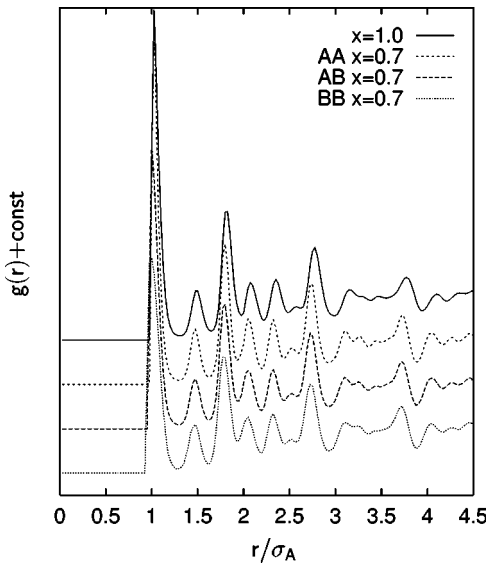

FIG. 7. Pair distribution functions $g_{AA}(r)$, $g_{AB}(r)$, and $g_{BB}(r)$ for the species A and B in a system with $\alpha=0.95$ and $x_A=0.7$ crystallized from a fluid phase by applying a pressure of $P_E\sigma_{AA}^3/(kT)=26.0$. Also shown in this figure is the pair distribution function of a single component system ($x=1.0$) at the same pressure.

For a size ratio of $\alpha=0.85$ crystallization is more hindered. We did not observe crystallization for pressure values below the pressure of the eutectic point at $x\approx0.26$, $P_E\sigma_{AA}^3/kT\approx23.0$ [24]. Crystallization was observed for a system with a mole fraction of $x_A=0.8$ and a pressure of $P_E=24.0$. Thus the point for which we found crystallization lies within the coexistence region of crystalline A and crystalline B but we did not see any sign of phase separation. The $g(r)$ functions for the crystalline system are shown in Fig. 9. The sharpness of the peak structure is distinctly reduced compared to that of the pure component system. Moreover, the functions $g_{AA}(r)$, $g_{AB}(r)$, and $g_{BB}(r)$ show mutually different structures, proving that now the two species are

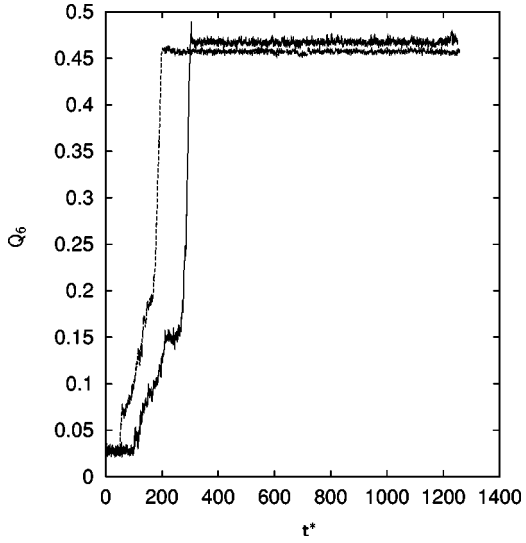

FIG. 8. Time dependence of the crystalline order parameter Q_6 as a function of time $t^*=t/(\sigma\sqrt{m/kT})$ for the binary mixture with $\alpha=0.95$, $x_A=0.7$, and $P_E\sigma_{AA}^3/(kT)=26.0$ (- - -) together with the one-component results at the same pressure with $P_E\sigma^3/(kT)=26.0$ (—), already used for the results in Fig. 7.

included in different ways in the crystallized structure. The system ends up in a partly crystallized metastable alloy of the two components, which is not demixing within the simulation time.

The phase diagram of the hard sphere system with $\alpha=0.73$ shows a eutectic point at $x\approx0.15$, $P_E\sigma_{AA}^3/kT\approx32.6$ [28]. For pressures between $P_E\sigma_{AA}^3/kT\approx11.2$ and $P_E\sigma_{AA}^3/kT\approx32.6$ phase regions are found where a fluid mixture coexists with a pure A or pure B crystal. We focused on

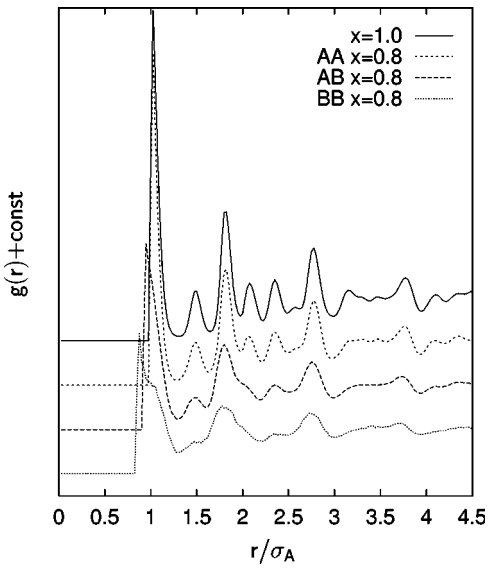

FIG. 9. Pair correlation functions $g_{AA}(r)$, $g_{AB}(r)$, and $g_{BB}(r)$ for the species A and B in a system with $\alpha=0.85$ and $x_A=0.8$ crystallized from a fluid phase by applying a pressure of $P_E\sigma_{AA}^3/(kT)=24.0$. Also shown in this figure is the pair correlation function of a single-component system ($x_A=1.0$) at the same pressure.

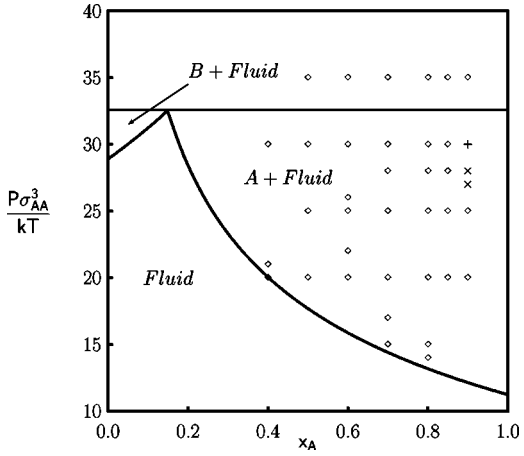

FIG. 10. Pressure versus composition phase diagram of binary hard sphere mixtures with $\alpha=0.73$ [28]. The ($\diamond$) symbols denote state points where no crystallization has been observed within the simulation runs. Crystallization was found for a systems of 864 spheres at the point denoted by (+) and for small size systems with 256 spheres at the points denoted by ($\times$).

the (crystal A + fluid) coexistence region that is distinctly more extended in the phase diagram than the (crystal B + fluid) phase coexistence region. In Fig. 10 the success of the crystallization attempts at different points in the phase diagram is noted. The only time we saw signs of crystallization for a system of 864 particles was for $P_E\sigma_{AA}^3/(kT)=28.0$, $x_A=0.9$, where there are only 10% of the species B left. Apparently, the mismatch of sphere sizes is so large that a joint crystallization is prevented, while, on the other hand, no phase separation sets in within the quenched system. So the systems remain in metastable fluid states. The fluid states are very well predicted by the equation of state of Mansoori *et al.* [43].

If α is decreased further the phase diagrams become more complex as crystalline phases with substitutional order such as AB, AB_2, and AB_{13} become stable. The hard sphere phase diagram for $\alpha=0.43$ includes stable crystal A, crystal B, and crystal AB_2 phases [28,27]. For pressures lower than $P_E\sigma_{AA}^3/kT=72.8$ only a fluid phase region and a coexistence region of crystal A and fluid exist. In the coexistence region a phase separation process starting from an AB crystal was observed in a previous work by Trizac *et al.* [27]. We have performed some N-P-T simulation runs for this size ratio with $x=0.8$ and $P_E\sigma_{AA}^3/kT=28.0$. In all simulation runs the crystalline order parameter increases until it reaches a value of $Q_6\approx0.28$. If we consider that due to the lever rule the system should consist of a crystal fraction and a fluid fraction in a mole ratio of about 2:5, the crystalline order parameter $Q_6\approx0.28$ is surprisingly high. From the theory it is expected that the crystalline A phase and the mixed fluid phase should phase separate. At the end of the simulation run no distinct separation could be observed. However, a certain coagulation of the B species was found. Spheres of species A and B form regions with low crystalline order that enclose regions of pure A crystals. The effect is rather weak but the coagulation can be detected indirectly. By taking the distance of randomly included test points in the simulation volume to

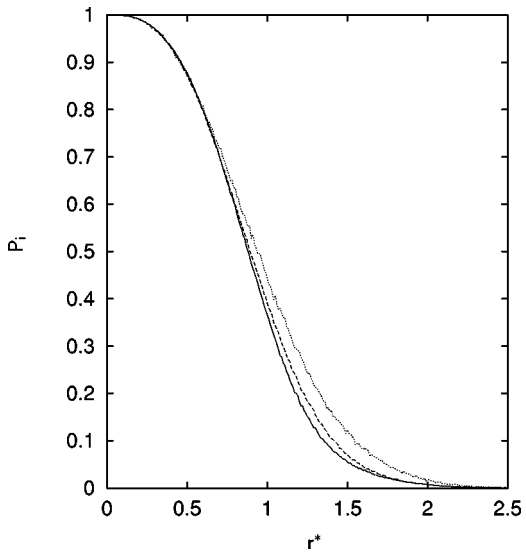

FIG. 11. The function $P_i(r)$ at three stages during a pressure quench of a binary system with $\alpha=0.43$, $x_A=0.8$, and $P_E\sigma_{AA}^3/(kT)=28.0$. The three curves correspond to reduced times: $t^*=30.0$ (—), $t^*=600.0$ (- - -), and $t^*=1200.0$ ($\cdots$).

the center of mass of the nearest *B* component sphere, one can characterize the space not occupied by the species *B*. Figure 11 shows the probability $P_i(r)$ that the distance between a randomly inserted point and the nearest B component sphere is larger than *r*. This is equivalent to the function $E_v(r)$ defined by Torquato and coworkers [44] in their formal treatment of nearest neighbor distributions in assemblies of spherical particles. A tendency toward coagulation of the B particles is detected sensitively by a shift of $P_i(r)$ towards higher values of *r*. In Fig. 11 functions $P_i(r)$ are shown for configurations taken in the fluid state ($t^*=30.0$), for a state shortly after Q_6 has approached its final value ($t^*=600.0$) and for a state at the end of the simulation ($t^*=1200.0$). The latter curve is shifted towards higher values of *r*, indicating that, to some extent, a phase separation process is initiated after the crystallization has set in. This effect was reproduced in several independent runs but an ongoing phase separation process beyond the effect shown in Fig. 11 could not be found on the time scales accessible in the current simulations.

V. CONCLUSIONS

In this paper we have presented a study of the crystallization dynamics in hard sphere systems. The *NPT* ensemble simulation technique enables us to mimic the response of a low density system on a quenching process. This can be performed in a one-step process without the need of artificial preparations of high density fluid states. It proves to be an excellent tool to investigate the dynamics of crystal order formation in hard sphere systems.

The metastable fluid branch in the hard sphere phase diagram of one-component systems could be reproduced in the *NPT* ensemble proving that the metastability is not caused by the *NVE* ensemble in which any fluctuations of the overall density are omitted. The metastable branch as obtained in previous *NVE* ensemble simulations could be reproduced within the accuracy of the method. However, no additional evidence was found for the existence of a thermodynamic glass transition within the metastable fluid branch.

For one-component systems crystallization was frequently observed in the pressure region $20.0\leqslant P_E\sigma_{AA}^3/kT\leqslant 30.0$. As the system crosses the metastable branch, density and order parameter increases are correlated showing a small increase in the region of the metastable state followed by one or several sudden increases ending up at a value that stays rather constant during the rest of the simulation run. The process confirms the dynamics in the *NVE* ensemble, where it is the pressure that changes slowly in the vicinity of the metastable branch and then drops rather quickly towards a final value. At the same time as crystallization sets in, the amount of fcc clusters within the system starts to increase continuously. This process, however, goes on after the growth of Q_6 has come to an end. The fcc order arises from an already dense system. The growth of fcc order typically starts from small fcc cluster seeds transferring their fcc order on neighboring non-fcc clusters without changing the overall density of the system.

The degree to which it is possible to observe crystallization in mixtures of hard spheres depends on the size ratio α. For α greater than about 0.73, crystallization becomes more difficult as the size ratio decreases from unity. This is associated with the fact that crystallization involves a change in composition as well as translational order. As would be expected, for size ratios close to unity, where the stable solid state is a substitutionally disordered solid solution the behavior is similar to that seen for single component systems. For $\alpha=0.85$ we also found crystallization into a substitutionally disordered solid solution for a state where this is metastable with respect to solid-solid phase separation [24]. Once the solid phase has formed the process of equilibrating, the composition distribution becomes too slow to be observed on the time scale of these simulations. If the size ratio is as small as $\alpha=0.43$, crystallization takes place more easily again. In the coexistence region of the *A* crystal and a fluid the *A* species starts to form crystalline structures. The small spheres of the *B* species are now small enough to escape from the crystal formation and show a tendency to coagulate in fluid regions together with a part of the *A* component. In between the fluid regions, well crystallized fractions of pure *A* crystals exist. This result is in accordance with simulation results by Trizac *et al.* [27] and gives additional insights into the mechanism and the sequence of the crystallization and the phase separation processes. At first, formation of crystalline order takes place between the large spheres, which is accompanied by a distinct increase in the density. Then the system tends to initiate a phase separation process as the development of crystalline order between the *A* component spheres continues. Our results for mixtures give an idea of the kind of

results that can be obtained from the present approach, but they are somewhat preliminary. It is hoped that future work with larger system sizes and longer runs should lead to more definitive conclusions.

ACKNOWLEDGMENTS

This work was supported by a grant from the U.S. Department of Energy (Contract No. DE-FG02-90ER14150).

[1] B.J. Alder and T.E. Wainwright, J. Chem. Phys. **27**, 1208 (1957).
[2] B.J. Alder and T.E. Wainwright, J. Chem. Phys. **31**, 459 (1959).
[3] W.G. Hoover and F.H. Ree, J. Chem. Phys. **47**, 4873 (1967).
[4] W.G. Hoover and F.H. Ree, J. Chem. Phys. **49**, 3609 (1968).
[5] H. Reiss and A.D. Hammerich, J. Phys. Chem. **90**, 6252 (1986).
[6] P.A. Monson and D.A. Kofke, Adv. Chem. Phys. **115**, 113 (2000).
[7] P.N. Pusey, in *Liquids Freezing and the Glass Transition*, edited by J.P. Hansen, D. Leveesque, and J. Zinn-Justin (Elsevier, Amsterdam, 1991), p. 763.
[8] D. Frenkel and A.J.C. Ladd, J. Chem. Phys. **81**, 3188 (1984).
[9] L.V. Woodcock, Nature (London) **384**, 141 (1997).
[10] S. Pronk and D. Frenkel, J. Chem. Phys. **110**, 4589 (1999).
[11] A.D. Bruce, A.N. Jackson, G.J. Ackland, and N.B. Wilding, Phys. Rev. E **61**, 906 (2000).
[12] N.F. Carnahan and K.E. Starling, J. Chem. Phys. **51**, 635 (1969).
[13] S. Torquato, T.M. Truskett, and P.G. Debenedetti, Phys. Rev. Lett. **84**, 2064 (2000).
[14] R.J. Speedy, J. Chem. Phys. **100**, 6684 (1994).
[15] M.D. Rintoul and S. Torquato, Phys. Rev. Lett. **77**, 4198 (1996).
[16] M.D. Rintoul and S. Torquato, J. Chem. Phys. **105**, 9258 (1996); **107**, 2698 (1997).
[17] S. Torquato, Nature (London) **405**, 521 (2000).
[18] R.J. Speedy, J. Phys.: Condens. Matter **9**, 8591 (1997).
[19] R.J. Speedy, Mol. Phys. **95**, 169 (1998).
[20] M.D. Rintoul and S. Torquato, Phys. Rev. E **58**, 532 (1998).
[21] P. Richard, L. Oger, J.-P. Troadec, and A. Gervois, Phys. Rev. E **60**, 4551 (1999).
[22] T.M. Truskett, S. Torquato, and P.G. Debenedetti, Phys. Rev. E **62**, 993 (2000).
[23] K. Kendall, C. Stainton, F. van Swol, and L.V. Woodcock, Int. J. Thermophys. (to be published).
[24] W.G.T. Kranendonk and D. Frenkel, Mol. Phys. **72**, 715 (1991); **72**, 679 (1991); **72**, 699 (1991)
[25] M.D. Eldridge, M.A. Madden, and D. Frenkel, Mol. Phys. **80**, 987 (1993).
[26] M.D. Eldridge, P.A. Madden, P.N. Pusey, and P. Bartlett, Mol. Phys. **84**, 395 (1995).
[27] E. Trizac, M.D. Eldridge, and P.A. Madden, Mol. Phys. **90**, 675 (1997).
[28] X. Cottin and P.A. Monson, J. Chem. Phys. **102**, 3354 (1995).
[29] G. Jackson, J.S. Rowlinson, and F. van Swol, J. Phys. Chem. **91**, 4907 (1987)
[30] W.S. Jodrey and E.M. Tory, Phys. Rev. A **32**, 2347 (1985).
[31] A.S. Clarke and J.D. Wiley, Phys. Rev. B **35**, 7350 (1987).
[32] B.D. Lubachevsky and F.H. Stillinger, J. Stat. Phys. **60**, 561 (1990).
[33] M.P. Allen and D.J. Tildesley, *Computer Simulation of Liquids* (Clarendon Press, Oxford, 1987).
[34] D. Frenkel and B. Smit, *Understanding Molecular Simulation* (Academic Press, San Diego, 1987).
[35] H.C. Andersen, J. Chem. Phys. **72**, 2384 (1980).
[36] Ph. de Smedt, J. Talbot, and J.L. Lebowitz, Mol. Phys. **59**, 625 (1986).
[37] T. Gruhn and P. Monson, Phys. Rev. E **63**, 061106 (2001).
[38] G.F. Voronoï and J. Reine, Angew. Math. **134**, 198 (1908).
[39] W. Brostow, M. Chybicki, R. Laskowski, and J. Rybicki, Phys. Rev. B **57**, 13 448 (1998).
[40] P.J. Steinhardt, D.R. Nelson, and M. Ronchetti, Phys. Rev. B **28**, 784 (1983).
[41] H. Gades and A.C. Mitus, Physica A **176**, 297 (1991).
[42] A.C. Mitus, F. Smolej, H. Hahn, and A.Z. Patashinski, Europhys. Lett. **32**, 777 (1995).
[43] G.A. Mansoori, N.F. Carnahan, K.E. Starling, and T.W. Leland Jr., J. Chem. Phys. **54**, 1523 (1971).
[44] S. Torquato, B. Lu, and J. Rubinstein, Phys. Rev. A **41**, 2059 (1990).